Nigerian Journal of Physics (NJP)
ISSN online: 3027-0936
ISSN print: 1595-0611
DOI: https://doi.org/10.62292/njp.v35(s).2026.732
Volume 35(S), 2026

Critical Interface Defect Density Governing Thermodynamic Losses and Photovoltaic Performance in $FASnI_3$ Perovskite Solar Cells

***[1]Ejikeme Ezo Igbokwe, [2]Elizabeth Chinyere Nwaokorongwu and [2]Uchechi Patricia Okpechi - Kanayochukwu**

[1]Department of Physics with Electronics, Ogbonnaya Onu Polytechnic, Aba, Nigeria.
[2]Department of Physics, Michael Okpara University of Agriculture, Umudike, Nigeria.

*Corresponding Author's Email: ejikeme.igbokwe@ogbonnayaonupolytechnic.edu.ng

Keywords:
Entropy-Generation Index, $FASnI_3$, Interface Defects, Perovskite Solar Cells, SCAPS-1D, Temperature Effects

Submitted: 02 July 2026

Accepted: 17 July 2026

Published: 16 Sept. 2026

ABSTRACT

Lead-free formamidinium tin iodide ($FASnI_3$) perovskite solar cells are promising alternatives to lead-based devices, but their performance is limited by interface defect-assisted recombination and thermal instability. Although SCAPS-1D has been widely used to optimize these devices, the combined effects of operating temperature and interface defect density on both photovoltaic and thermodynamic performance remain insufficiently understood. In this study, SCAPS-1D was employed to investigate the coupled influence of operating temperature (300–400 K) and $SnO_2/FASnI_3$ interface defect density (10^8–10^{18} cm^{-2}) on a Front contact/$SnO_2/FASnI_3$/CuI/Back contact perovskite solar cell under AM1.5G illumination (100 mW cm^{-2}). Conventional photovoltaic parameters (Voc, Jsc, FF, and PCE) were evaluated alongside power loss and a normalized Entropy-Generation Index (EGI) to quantify irreversible energy dissipation. The optimized baseline device achieved a Voc of 1.00 V, Jsc of 28.52 mA cm^{-2}, FF of 70.81%, and PCE of 20.30%. The device exhibited good thermal tolerance, maintaining efficiencies close to 20% over the investigated temperature range, with only a 3.13% reduction between the maximum efficiency and that at 400 K. In contrast, interface defect density had a much stronger impact on performance. The PCE remained nearly constant below 10^{15} cm^{-2} but declined rapidly at higher defect densities because of enhanced Shockley–Read–Hall recombination. Corresponding increases in power loss and changes in the normalized EGI identified 10^{15} cm^{-2} as the critical $SnO_2/FASnI_3$ interface defect threshold. These findings highlight interface quality as the dominant factor governing the efficiency and thermodynamic stability of lead-free $FASnI_3$ perovskite solar cells.

INTRODUCTION

Perovskite solar cells (PSCs) have emerged as one of the fastest-growing photovoltaic technologies because of their exceptional optoelectronic properties, including high optical absorption coefficients, long carrier diffusion lengths, tunable bandgaps, and solution-processable fabrication. Since the pioneering work of Kojima et al. (2009), the certified power conversion efficiency (PCE) of PSCs has increased from 3.8% to over 27%, demonstrating their potential as an alternative to conventional crystalline silicon solar cells (Kojima et al., 2009; Green et al., 2025). Despite this rapid progress, concerns regarding the toxicity of lead (Pb) and the long-term operational stability of lead-based perovskites continue to hinder large-scale commercialization.

Recent reviews have highlighted the rapid improvement in photovoltaic technologies, emphasizing the central role of material engineering, interface optimization, and defect management in achieving high power conversion efficiencies across emerging solar-cell technologies (Ho et al., 2025; Zhang et al., 2026; AlZohbi, 2026; Amusan et al., 2019).

To overcome these challenges, significant research efforts have focused on lead-free tin-based perovskites. Among these materials, formamidinium tin iodide ($FASnI_3$) has attracted considerable attention owing to its direct bandgap (~1.4 eV), high absorption coefficient, excellent charge-carrier mobility, and low exciton binding energy, all of which are desirable for high-efficiency photovoltaic applications (Savill et al., 2021;

Wang et al., 2021; Zhang et al., 2018). Furthermore, $FASnI_3$ exhibits superior thermal and structural stability compared with methylammonium tin iodide ($MASnI_3$) (Ke & Kanatzidis, 2019; Wang et al., 2021), making it one of the most promising lead-free absorber materials for environmentally benign perovskite solar cells. Structurally, the larger ionic radius of the formamidinium (FA^+) cation optimizes the Goldschmidt tolerance factor closer to 1, which better stabilizes the 3D corner-sharing SnI_6 octahedral network and suppresses detrimental phase transitions. Thermally, $FASnI_3$ maintains its stuctural integrity and resists decomposition up to approximately 200 °C, whereas $MASnI_3$ suffers from severe Sn^{2+} to Sn^{4+} oxidation and begins to rapidly degrade at much lower operational temperatures, often below 100 °C (Ke & Kanatzidis, 2019; Peng & Xie 2020).

However, the practical performance of $FASnI_3$ solar cells remains below that of their lead-based counterparts. The primary limitation arises from the spontaneous oxidation of Sn^{2+} to Sn^{4+}, which produces high intrinsic carrier concentrations and abundant defect states. These defects act as Shockley–Read–Hall (SRH) recombination centers, resulting in increased non-radiative recombination, reduced open-circuit voltage, and accelerated device degradation (Yao et al., 2020; Ke et al., 2018).

Among the various loss mechanisms, interface defects have been recognized as one of the most significant factors limiting the efficiency and stability of PSCs. Defects located at the electron transport layer (ETL)/absorber and absorber/hole transport layer (HTL) interfaces create trap-assisted recombination pathways, impede charge extraction, and increase carrier losses (Abbas et al., 2024; Wang et al., 2024; Wu et al., 2021). Consequently, interface engineering through defect passivation, transport-layer optimization, and energy-band alignment has become an effective strategy for improving photovoltaic performance and long-term stability (Li et al., 2026; Noman et al., 2024).

Becuse systematic experimental optimization is both expensive and time-consuming, numerical simulation has become an indispensable tool for device design. The Solar Cell Capacitance Simulator (SCAPS-1D) has been extensively employed to investigate the effects of material properties, defect states, transport layers, and operating conditions on perovskite solar-cell performance, providing valuable insights before experimental fabrication (Burgelman et al., 2004; Burgelman et al., 2000).

Several studies have examined the influence of operating temperature on tin-based perovskite solar cells using SCAPS-1D. Increasing temperature generally reduces the open-circuit voltage due to the rise in intrinsic carrier concentration and reverse saturation current, whereas the short-circuit current density changes only slightly. As a result, the overall power conversion efficiency declines at elevated temperatures because of enhanced non-radiative recombination and increased thermal losses (Igbokwe et al., 2026; Ho et al., 2025).

Similarly, numerous investigations have demonstrated that interface defects strongly influence the photovoltaic performance of PSCs. Increasing interface defect density enhances SRH recombination, leading to reductions in the open-circuit voltage, fill factor, and overall conversion efficiency. Previous SCAPS-based studies have therefore focused on reducing interface defects through transport-layer selection, interface passivation, and optimization of capture cross-sections to improve carrier extraction and suppress non-radiative recombination (Izadi et al., 2020; Alqurashi, 2024). For example, simulations using tin dioxide (SnO_2) as the electron transport layer (ETL) and copper thiocyanate (CuSCN) as the hole transport layer (HTL) have demonstrated that optimizing layer thicknesses minimizes defect densities and significantly enhances electron and hole mobilities at the interfaces (Hanif et al., 2024). Furthermore, extensive device modeling has evaluated various lead-free architectures, such as replacing standard transport layers with zinc phosphide (Zn_3P_2) for the HTL and tungsten disulfide (WS_2) for the ETL, which improves band alignment with the absorber layer and drastically mitigates trap-assisted voltage losses (Islam et al., 2026).

For $FASnI_3$ devices specifically, recent simulation studies have mainly investigated the influence of hole transport materials, absorber thickness, bulk defect density, back-contact work function, and optical losses on device performance. These studies, such as the Al/ETL/$FASnI_3$/GO/Au configuration, have successfully improved simulated efficiencies through parameter optimization but have generally treated temperature and interface defect density as independent variables (Alqurashi, 2024).

Although temperature and interface defects are individually recognized as critical factors governing the performance of tin-based perovskite solar cells, their coupled influence has received comparatively little attention. Most published SCAPS investigations vary either operating temperature or interface defect density independently, making it difficult to understand how thermal stress modifies interface defect tolerance and the onset of recombination-induced degradation (Abdulsalam & Lariski, 2026; Afrin et al., 2024). Furthermore, a critical interface defect density beyond which $FASnI_3$ solar cells transition from defect-tolerant to defect-dominated operation has not been clearly established.

Although thickness-dependent recombination has recently been investigated in $FASnI_3$ solar cells, the combined influence of interface defect density and operating temperature has not yet been systematically

examined (Khan & Al Ahmed, 2024; El Arfaoui et al., 2023; Abdelaziz et al., 2020). The present work therefore extends previous studies by identifying a thermodynamic critical interface defect threshold using coupled photovoltaic and entropy-generation analyses.

To address this gap, the present study employs a two-parameter SCAPS-1D simulation to investigate the combined effects of operating temperature and SnO_2/$FASnI_3$ interface defect density on the photovoltaic performance of $FASnI_3$ perovskite solar cells. The study aims to identify the critical interface defect threshold governing thermal degradation and to provide practical design guidelines for developing efficient and thermally stable lead-free perovskite solar cells.

MATERIALS AND METHODS

Device Architecture

The photovoltaic device investigated in this study consists of a planar n–i–p heterojunction architecture comprising Front contact, tin oxide (SnO_2), formamidinium tin iodide ($FASnI_3$), copper iodide (CuI), and a back contact. SnO_2 was employed as the electron transport layer (ETL) because of its high optical transparency, excellent electron mobility, suitable conduction-band alignment, and good chemical stability. $FASnI_3$ served as the photoactive absorber layer owing to its direct bandgap of approximately 1.41 eV and high absorption coefficient across the visible spectrum. Copper iodide (CuI) was selected as the hole transport layer (HTL) due to its high hole mobility, wide bandgap, and favourable valence-band alignment with $FASnI_3$, thereby facilitating efficient hole extraction while suppressing electron back transfer.

The simulated device architecture was therefore configured as:

Front Contact/SnO_2/$FASnI_3$/CuI/Back Contact

Where Front contact and Back contact function as the front and back Ohmic contacts, respectively. Photogenerated electrons are transported through the SnO_2 layer towards the front contact, whereas holes are extracted through the CuI layer to the back contact. The energy-level alignment between these layers promotes efficient charge separation while minimizing interface recombination losses. The schematic illustration of the simulated perovskite solar cell architecture is displayed in Figure 1.

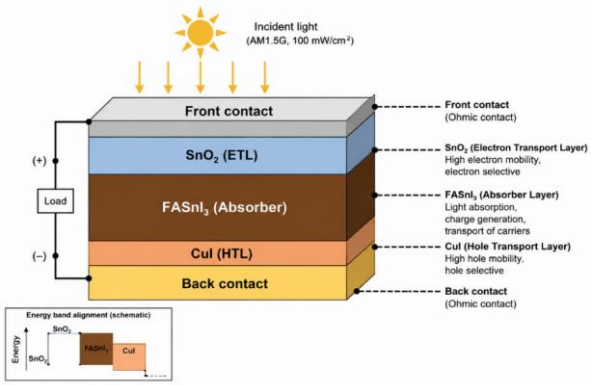

Figure 1: Schematic Illustration of the Simulated Perovskite Solar Cell Architecture

SCAPS Simulation Parameters

The numerical simulations were performed using SCAPS-1D Version 3.3.12 (ELIS-UGent, Belgium). SCAPS solves the coupled Poisson equation together with the electron and hole continuity equations using a finite-difference approach to simulate carrier transport and recombination in multilayer thin-film solar cells (Burgelman et al., 2004; Burgelman et al., 2000).

All simulations were carried out under standard test conditions using the AM1.5G solar spectrum with an incident power density of 100 mW cm^{-2} (1 Sun). Optical generation was calculated internally by SCAPS using the absorption coefficients specified for each semiconductor layer. The neutral-density filter transmission was maintained at 100%, while the operating frequency was fixed at 1 MHz. SCAPS numerical convergence settings were adopted with a voltage step size of 0.02 V during current density–voltage (J–V) calculations.

The material properties for each semiconductor layer, including thickness, bandgap, electron affinity, dielectric constant, carrier mobilities, effective density of states, doping concentration, and defect parameters, were

obtained from experimentally validated literature and implemented in the SCAPS device definition file The selected values have been widely validated for modeling lead-free $FASnI_3$ perovskite solar cells (Burgelman et al., 2004; Alqurashi, 2024; Ke et al., 2018; Igbokwe et al., 2026). These parameters are summarized in Table 1.

Table 1: Material Parameters Used for the SCAPS-1D Simulation of the SnO_2/$FASnI_3$/CuI Perovskite Solar Cell

Parameter	SnO_2 (ETL)	$FASnI_3$ Absorber	CuI (HTL)	Unit
Thickness	200	500	200	Nm
Bandgap (Eg)	3.60	1.41	2.98	eV
Electron affinity (χ)	4.00	4.17	2.10	eV
Relative dielectric constant (εr)	9.0	8.2	6.5	—
Electron effective density of states (Nc)	2.2×10^{24}	1.0×10^{24}	2.8×10^{25}	m^{-3}
Hole effective density of states (Nv)	1.8×10^{25}	1.0×10^{24}	1.0×10^{25}	m^{-3}
Electron mobility (μn)	1.0×10^{-2}	4.0×10^{-4}	1.0×10^{-4}	$m^2\ V^{-1}\ s^{-1}$
Hole mobility (μp)	1.0×10^{-3}	5.0×10^{-4}	2.0×10^{-3}	$m^2\ V^{-1}\ s^{-1}$
Donor concentration (Nd)	1.0×10^{23}	0	0	m^{-3}
Acceptor concentration (Na)	0	0	1.0×10^{25}	m^{-3}
Bulk defect density (Nt)	1.0×10^{21}	5.0×10^{20}	1.0×10^{20}	m^{-3}
Electron capture cross-section (σn)	1.0×10^{-19}	1.0×10^{-19}	1.0×10^{-19}	m^2
Hole capture cross-section (σp)	1.0×10^{-19}	1.0×10^{-19}	1.0×10^{-19}	m^2

Simulation Procedure

The simulation procedure consisted of four sequential stages: model validation, temperature analysis, interface defect analysis, and coupled parameter investigation.

Initially, the baseline Front contact/SnO_2/$FASnI_3$/CuI/Back contact device was simulated under standard operating conditions (300 K and AM1.5G illumination) to obtain the reference photovoltaic characteristics, including the open-circuit voltage (Voc), short-circuit current density (Jsc), fill factor (FF), maximum power point (MPP), and power conversion efficiency (PCE). The optimized baseline device served as the reference for all subsequent simulations.

To investigate the influence of operating temperature, the device temperature was varied linearly from 300 K to 400 K in increments of 25 K while maintaining all material properties constant. This enabled the evaluation of the thermal stability of the optimized device.

Subsequently, the total defect density at the SnO_2/$FASnI_3$ interface was varied logarithmically from 10^8 to 10^{18} cm^{-2} while all other parameters remained unchanged. This range was selected to investigate the transition from defect-tolerant behaviour to severe recombination-induced performance degradation.

Finally, a two-parameter batch simulation was performed by simultaneously varying both the operating temperature and the interface defect density. The batch analysis generated a total of 50 independent simulations (5 temperatures × 10 interface defect densities), allowing the coupled influence of thermal stress and interface defects on the photovoltaic performance of the $FASnI_3$ solar cell to be systematically investigated.

The principal photovoltaic parameters extracted from each simulation included the open-circuit voltage (Voc), short-circuit current density (Jsc), fill factor (FF), maximum power point voltage (VMPP), maximum power point current density (JMPP), and power conversion efficiency (PCE). The complete simulation conditions are summarized in Table 2.

Table 2: Simulation Parameters and Batch Conditions Employed in the Two-Parameter SCAPS-1D Study

Parameter	Value
Simulation software	SCAPS-1D Version 3.3.12
Device architecture	SnO_2/$FASnI_3$/CuI
Illumination spectrum	AM1.5G
Incident power density	100 mW cm^{-2}
Optical generation	Internal SCAPS calculation
Neutral density filter	100% transmission
Temperature range	300–400 K
Temperature step	25 K
Interface investigated	SnO_2/$FASnI_3$
Interface defect density	10^8–10^{18} cm^{-2}
Defect density spacing	Logarithmic

Parameter	Value
Defect energy level	0.60 eV
Electron capture cross-section	1×10^{-23} m²
Hole capture cross-section	1×10^{-23} m²
Voltage step	0.02 V
Frequency	1 MHz
Series resistance	1×10^{-9} Ω m²
Front contact work function	5.20 eV
Back contact work function	4.40 eV
Number of temperatures	5
Number of interface defect densities	11
Total simulations	50

Data Analysis

The photovoltaic performance of the simulated devices was evaluated using the current density–voltage (J–V) characteristics generated by SCAPS. The power conversion efficiency (PCE) was determined from

$$\eta = \frac{V_{OC} \times J_{SC} \times FF}{P_{in}} \times 100 \quad (1)$$

where (V_{OC}) is the open-circuit voltage (V), (J_{SC}) is the short-circuit current density (mA cm⁻²), (FF) is the fill factor, and (P_{in}) is the incident solar power density (100 mW cm⁻²).

The maximum output power density (P_{max}) was calculated using the maximum power point parameters obtained from SCAPS according to

$$P_{max} = V_{MPP} \times J_{MPP} \quad (2)$$

where (V_{MPP}) and (J_{MPP}) represent the voltage and current density at the maximum power point, respectively.

The power loss during photovoltaic conversion was estimated as

$$P_{loss} = P_{in} - P_{max} \quad (3)$$

To complement the conventional photovoltaic analysis, a normalized entropy-generation index (EGI) was evaluated as

$$EGI = \frac{P_{loss}}{T} \quad (4)$$

where (T) is the operating temperature in Kelvin. This parameter was employed as a normalized indicator of thermodynamic irreversibility and was used to compare relative energy losses under different operating temperatures and interface defect densities. It should be noted that the EGI represents a comparative performance metric rather than the absolute thermodynamic entropy generation of the device.

The calculated photovoltaic and thermodynamic parameters were exported to Microsoft Excel for post-processing, graphical visualization, and comparative analysis. Variations in PCE, Voc, Jsc, FF, power loss, and the normalized entropy-generation index were analysed as functions of operating temperature and SnO_2/$FASnI_3$ interface defect density to identify the critical defect threshold governing the transition from defect-tolerant to defect-dominated operation.

RESULTS AND DISCUSSION

Validation of the Baseline Device

Before investigating the effects of temperature and interface defect density, The Front contact/SnO_2/$FASnI_3$/CuI/Back contact perovskite solar cell was simulated under standard test conditions (AM1.5G illumination, 100 mW cm⁻², 300 K) to establish a baseline for subsequent analyses. The simulated photovoltaic parameters are presented in Table 3.

The optimized baseline device achieved a Voc of 1.00 V, Jsc of 28.51 mA cm⁻², FF of 70.81%, and a PCE of 20.30%, with a maximum power point of 0.78 V and 26.02 mA cm⁻². These values are comparable to those reported for optimized lead-free $FASnI_3$ perovskite solar cells in previous SCAPS studies, confirming the reliability of the adopted simulation parameters.

The relatively high Voc indicates low interfacial recombination, while the large Jsc reflects efficient light absorption and carrier generation. The fill factor above 70% further suggests effective carrier transport with minimal resistive losses. Consequently, the validated baseline provides a reliable reference for evaluating the effects of temperature and SnO_2/$FASnI_3$ interface defect density on photovoltaic performance, power loss, and the normalized entropy-generation index (EGI).

Table 3: Photovoltaic Performance of the Optimized Baseline SnO_2/$FASnI_3$/CuI/ Perovskite Solar Cell Under Standard AM1.5G Illumination (100 mW cm^{-2}) at 300 K

Parameter	Value	Unit
Open-circuit voltage	1.0051	V
Short-circuit current density	28.5199	mA cm^{-2}
Fill factor	70.8073	%
Maximum power point voltage	0.7800	V
Maximum power point current density	26.0219	mA cm^{-2}
Power conversion efficiency	20.2971	%

Effect of Temperature

The effect of operating temperature on the photovoltaic performance of the optimized Front contact/SnO_2/$FASnI_3$/CuI/Back contact perovskite solar cell was investigated by varying the temperature from 300 to 400 K, while keeping all other device parameters constant. The corresponding variations in Voc, Jsc, FF, and PCE are shown in Figure 2.

As shown in Figure 2(a), the open-circuit voltage decreases steadily from 1.0051 V at 300 K to 0.93 V at 400 K (≈7.3% reduction). This decline is attributed to increased thermal recombination and a higher reverse saturation current, which reduce the quasi-Fermi level splitting (Alahmad, 2026; Abdelaziz et al., 2020).

In contrast, Jsc remains almost unchanged (≈28.51 mA cm^{-2}) throughout the temperature range (Figure 2(b)), This stability occurs because, within standard SCAPS-1D modeling environments, the material bandgap and optical absorption profile are treated as temperature-independent parameters. Consequently, the photogeneration rate of electron-hole pairs is solely dictated by the constant incident AM 1.5G illumination, leaving the short-circuit current largely unaffected by thermal fluctuations (Abdelaziz et al., 2020).

The fill factor increases gradually from 70.81% to 75.22% (Figure 2(c)), suggesting improved carrier transport under the adopted SCAPS simulation conditions, which partially compensates for the reduction in Voc. In this specific simulation architecture, this increase suggests that higher temperatures enhance the thermionic emission of carriers across the interfacial energy barriers at the SnO_2/$FASnI_3$ and $FASnI_3$/CuI junctions. This thermally activated transport effectively reduces the series resistance at the interfaces, thereby improving charge extraction and compensating for the reduction in V_{oc}. However, this simulated behavior sharply contrasts with typical experimental observations and modeling of other materials, such as standard $MAPbI_3$ or silicon solar cells. In physical experiments, the FF generally *decreases* at elevated temperatures due to increased electron-phonon scattering (which degrades bulk carrier mobility) and temperature-induced material degradation, both of which increase bulk series resistance and amplify non-radiative recombination (Nelson, 2003; Meng et al., 2021). This divergence highlights a limitation in standard static modeling, where thermally activated interfacial transport can overshadow the bulk mobility degradation typically experienced by physical devices.Consequently, the PCE increases slightly from 20.30% at 300 K to a maximum of 20.63% at 350 K, before decreasing to 19.98% at 400 K (Figure 2(d)). This indicates an optimum operating temperature of approximately 350 K, beyond which thermally activated recombination becomes the dominant loss mechanism.

The decrease in efficiency from the peak value to 400 K is approximately 3.13%, calculated as:

Percentage decrease$= \frac{20.6268-19.9816}{20.6268} \times 100 = 3.13\%$

Although this reduction is relatively small, it indicates that the device does not maintain perfectly constant performance with increasing temperature. Instead, the results suggest good thermal tolerance, with the fill factor partially compensating for the temperature-induced reduction in open-circuit voltage up to approximately 350 K. Beyond this temperature, thermally activated recombination becomes the dominant loss mechanism, resulting in a measurable decline in power conversion efficiency. Overall, the simulated $FASnI_3$ solar cell maintains stable photovoltaic performance throughout the investigated temperature range, maintaining an efficiency close to 20% across the investigated temperature range. However, the continuous reduction in Voc confirms that temperature-induced recombination ultimately limits device performance at elevated temperatures.

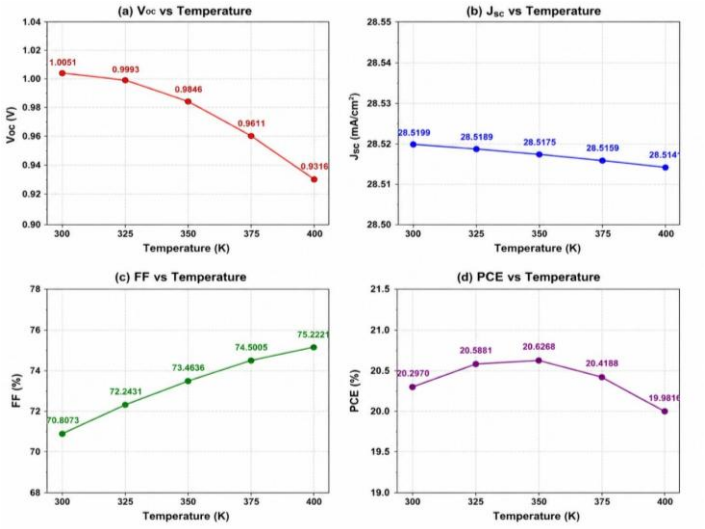

Figure 2: Variation of the Photovoltaic Parameters of the Optimized $FASnI_3$ Perovskite Solar Cell: (a) Open-Circuit Voltage (Voc), (b) Short-Circuit Current Density (Jsc), (c) Fill Factor (FF), and (d) Power Conversion Efficiency (PCE)

Combined Effect of Temperature and Interface Defect Density on Power Conversion Efficiency

The combined effects of operating temperature and $SnO_2/FASnI_3$ interface defect density on the power conversion efficiency (PCE) are presented in Figure 3(a–b). The results show that interface defect density has a much greater influence on device performance than temperature.

As shown in Figure 3(a), the PCE remains nearly constant (≈20–20.6%) for interface defect densities between 10^8 and 10^{14} cm^{-2} at all temperatures, indicating excellent defect tolerance and minimal recombination losses. However, once the defect density exceeds 10^{15} cm^{-2}, the efficiency decreases rapidly, reaching 14.54%, 14.20%, 13.79%, 13.36%, and 12.89% at 300, 325, 350, 375, and 400 K, respectively, for 10^{18} cm^{-2}. This sharp decline identifies 10^{15} cm^{-2} as the critical interface defect threshold, beyond which Shockley–Read–Hall recombination becomes the dominant loss mechanism.

The complementary trend in Figure 3(b) shows that, under low-defect conditions (10^8–10^{14} cm^{-2}), the PCE increases slightly with temperature and reaches a maximum of 20.63% at 350 K, before decreasing at higher temperatures. At higher interface defect densities ($\geq 10^{15}$ cm^{-2}), this beneficial temperature effect disappears, and the efficiency decreases progressively with increasing temperature due to enhanced carrier trapping and non-radiative recombination.

These results are broadly consistent with previous SCAPS studies, which reported that increasing interface defect density accelerates Shockley–Read–Hall recombination and reduces the photovoltaic performance of $FASnI_3$-based perovskite solar cells (Alqurashi, 2024; Igbokwe et al., 2026). However, unlike most published studies that reported a monotonic decrease in efficiency with increasing temperature (Abdelaziz et al., 2020; Ho et al., 2025), the present simulation predicts a slight efficiency enhancement up to 350 K under low-defect conditions. This behaviour suggests that thermally enhanced interfacial charge transport partially offsets thermal recombination losses before higher temperatures become detrimental.

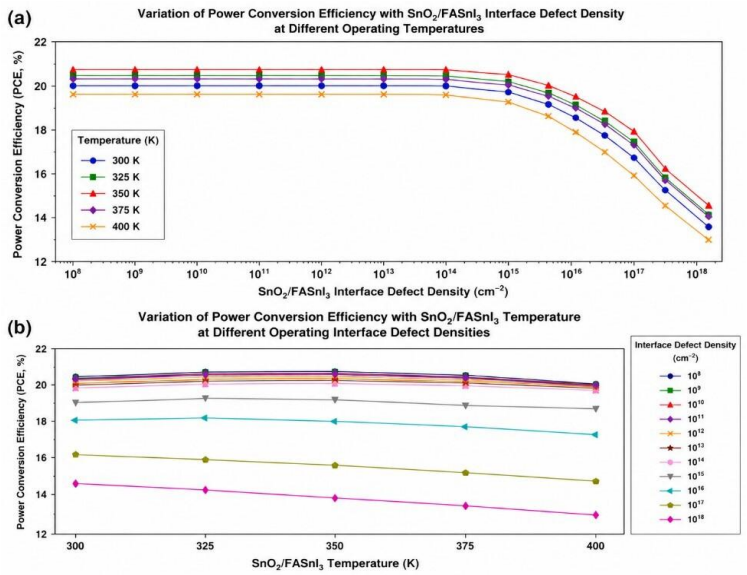

Figure 3: Combined Effects of Operating Temperature and SnO_2/$FASnI_3$ Interface Defect Density on the Power Conversion Efficiency (PCE)

Power Loss Analysis

The thermodynamic performance of the baseline Front contact/SnO_2/$FASnI_3$/CuI/Back contact perovskite solar cell was evaluated by analysing the power loss over the temperature range of 300–400 K under standard AM1.5G illumination. The calculated maximum output power, power loss, and normalized entropy-generation index (EGI) are presented in Table 4.

The maximum output power increases slightly from 20.29 mW cm^{-2} at 300 K to 20. mW cm^{-2} at 350 K, before decreasing to 19.98 mW cm^{-2} at 400 K. Accordingly, the power loss decreases from 79.70 mW cm^{-2} to a minimum of 79.37 mW cm^{-2} at 350 K, and then increases to 80.01 mW cm^{-2} at 400 K, producing the shallow U-shaped trend shown in Figure 4.

The minimum power loss at 350 K indicates the most efficient conversion of incident solar energy into electrical power, consistent with the maximum PCE observed at the same temperature. Above 350 K, thermally activated recombination increases irreversible energy dissipation, resulting in higher power losses. Although the overall variation is relatively small (about 0.65 mW cm^{-2}), the analysis identifies 350 K as the optimum operating temperature and provides a thermodynamic basis for the subsequent entropy-generation analysis.

Table 4: Calculated Power Loss and Normalized Entropy-Generation Index (EGI) of the Baseline Front Contact/SnO_2/$FASnI_3$/CuI/Back Contact Perovskite Solar Cell at Different Operating Temperatures

Temperature (K)	Pmax (mW cm^{-2})	Power Loss (mW cm^{-2})	EGI (mW cm^{-2} K^{-1})
300	20.2971	79.7029	0.2657
325	20.5881	79.4119	0.2443
350	20.6268	79.3732	0.2268
375	20.4188	79.5812	0.2122
400	19.9816	80.0184	0.2000

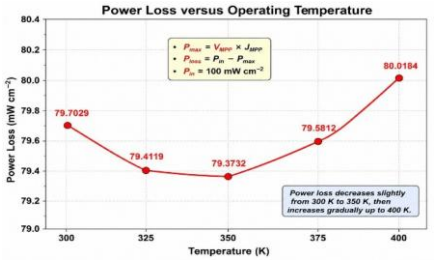

Figure 4: Variation of Power Loss with Operating Temperature for the Perovskite Solar Cell

The effect of SnO_2/$FASnI_3$ interface defect density on the power loss of the simulated perovskite solar cell was investigated over the range of 10^8–10^{18} cm^{-2} at operating temperatures of 300–400 K. The results are presented in Figure 5.

As shown in Figure 5, the power loss remains nearly constant for interface defect densities up to approximately 10^{14} cm^{-2}, indicating minimal recombination losses and effective charge collection. Beyond 10^{15} cm^{-2}, however, the power loss increases rapidly as Shockley–Read–Hall (SRH) recombination becomes significant. The deterioration is most pronounced between 10^{16} and 10^{18} cm^{-2}, where severe interface recombination substantially reduces the electrical power output.

Although operating temperature also affects power loss, its influence is much smaller than that of interface defect density. The power-loss curves remain closely grouped at low defect densities but diverge at $\geq 10^{16}$ cm^{-2}, showing that elevated temperatures intensify defect-assisted recombination and increase irreversible energy dissipation.

The transition from the defect-tolerant to the defect-dominated regime consistently occurs around 10^{15}–10^{16} cm^{-2} for all temperatures, confirming this range as the critical interface defect threshold. Overall, the results demonstrate that interface quality is the dominant factor controlling thermodynamic losses in the $FASnI_3$ solar cell, emphasizing the importance of effective interface passivation for maintaining high efficiency and low power loss.

The present results are consistent with recent SCAPS-based studies, which have identified interface defects as a primary source of Shockley–Read–Hall recombination, leading to increased power losses and reduced device efficiency (Abdulsalam & Lariski, 2026; Abbas et al., 2024; Alqurashi, 2024). Similar to these reports, the current study shows that power loss remains nearly constant at low interface defect densities but increases rapidly once the defect density exceeds approximately 10^{15} cm^{-2}. However, unlike previous studies that primarily evaluated photovoltaic parameters such as PCE, V_{OC}, and FF, the present work further quantifies thermodynamic losses through power-loss and normalized entropy-generation analyses, enabling the identification of a critical interface defect threshold (10^{15}–10^{16} cm^{-2}) that governs the transition from defect-tolerant to defect-dominated operation. This provides a more comprehensive framework for assessing interface quality and thermal reliability in lead-free $FASnI_3$ perovskite solar cells.

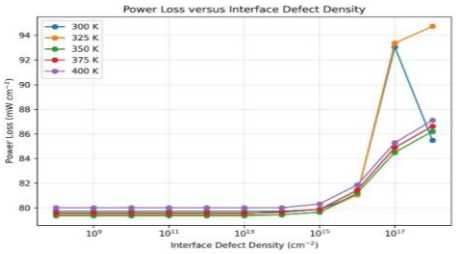

Figure 5**:** Variation of Power Loss with SnO_2/$FASnI_3$ Interface Defect Density at Different Operating Temperatures (300–400 K) under AM1.5G Illumination (100 mW cm^{-2})

Critical Interface Defect Threshold Identified from Photovoltaic and Thermodynamic Analyses

The combined photovoltaic and thermodynamic analyses reveal the existence of a well-defined critical interface defect threshold for the simulated Front contact/SnO_2/$FASnI_3$/CuI/Back contact perovskite solar cell. As summarized in Table 5, three distinct operating regimes can be identified according to the SnO_2/$FASnI_3$ interface defect density.

Table 5: Critical Interface Defect Threshold Identified from Photovoltaic and Thermodynamic Analyses

Interface defect regime	PCE behaviour	Power loss	Normalized EGI	Dominant mechanism
$\leq 10^{14}$ cm^{-2}	Stable (≈20–20.6%)	Nearly constant	Low	Effective charge collection with negligible interface recombination
$\approx 10^{15}$ cm^{-2}	Onset of degradation	Increasing	Increasing	Beginning of Shockley–Read–Hall (SRH) interface recombination
$\geq 10^{16}$ cm^{-2}	Rapid degradation	High	High	Defect-dominated non-radiative recombination and severe irreversible energy loss

The combined photovoltaic and thermodynamic analyses identify three distinct interface defect regimes. For defect densities below 10^{14} cm^{-2}, the device operates in a defect-tolerant region, maintaining a stable PCE of about 20–20.6%, with nearly constant power loss and low normalized entropy-generation index (EGI). This indicates effective charge collection and minimal irreversible energy dissipation.

As the interface defect density approaches 10^{15} cm^{-2}, the device begins to degrade. The PCE decreases while both power loss and EGI increase, marking the onset of significant Shockley–Read–Hall (SRH) recombination at the SnO_2/$FASnI_3$ interface. Since this transition occurs consistently across the investigated temperature range (300–400 K), 10^{15} cm^{-2} is identified as the critical interface defect threshold.

Above 10^{16} cm^{-2}, the device enters a defect-dominated regime characterized by a rapid drop in PCE and a sharp increase in power loss and EGI. This behaviour confirms that non-radiative recombination becomes the dominant loss mechanism, leading to greater thermodynamic irreversibility and reduced electrical output.

Overall, the results show that maintaining the interface defect density below ~10^{15} cm^{-2} is essential for achieving high efficiency, low entropy generation, and good thermal stability. This threshold provides a practical design guideline for interface engineering and passivation in high-performance lead-free $FASnI_3$ perovskite solar cells.

Entropy-Generation Index Analysis

Figure 6 shows the variation of the normalized Entropy-Generation Index (EGI) with SnO_2/$FASnI_3$ interface defect density at operating temperatures between 300 and 400 K. The EGI was used to assess the irreversible energy losses associated with interface recombination under different thermal conditions (Abdulsalam & Lariski, 2026; Abbas et al., 2024; Alqurashi, 2024).

At all temperatures, the EGI remains nearly constant for interface defect densities between 10^8 and 10^{14} cm^{-2}, indicating a defect-tolerant regime with effective charge collection and minimal irreversible losses. As the defect density approaches 10^{15} cm^{-2}, the EGI begins to change noticeably, coinciding with the decline in PCE, Voc, and FF. This behaviour marks the onset of significant Shockley–Read–Hall (SRH) recombination at the SnO_2/$FASnI_3$ interface.

Beyond 10^{16} cm^{-2}, the EGI decreases rapidly for all temperatures, reflecting severe degradation of photovoltaic performance due to increased non-radiative recombination. The simultaneous reduction in EGI and PCE confirms that excessive interface defects significantly reduce the fraction of incident solar energy converted into useful electrical power.

The results also show that the normalized EGI decreases with increasing operating temperature, with the highest values at 300 K and the lowest at 400 K. This trend is consistent with the definition of the normalized EGI, where temperature appears in the denominator, making it a useful metric for comparing thermodynamic losses under different operating conditions rather than representing the absolute entropy generation (Moot et al., 2021; Lin & Ravindra, 2020).

Overall, the combined thermodynamic and photovoltaic analyses identify ~10^{15} cm^{-2} as the critical interface defect threshold. Below this value, the device maintains stable performance and low irreversible losses, whereas above it, defect-assisted recombination dominates. The normalized EGI therefore provides a valuable thermodynamic indicator for evaluating interface quality and optimizing lead-free $FASnI_3$ perovskite solar cells.

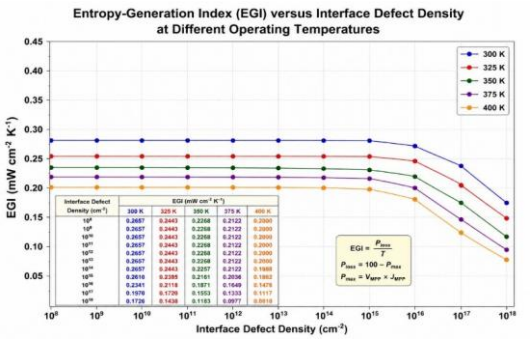

Figure 6: Variation of the Normalized Entropy-Generation Index (EGI) with SnO_2/$FASnI_3$ Interface Defect Density at Operating Temperatures Between 300 and 400 K

Figure 7 shows that the normalized entropy-generation index (EGI) decreases with increasing operating temperature for all investigated SnO_2/$FASnI_3$ interface defect densities. At low defect densities (10^8–10^{14} cm^{-2}), the EGI curves are almost identical, indicating minimal irreversible energy losses and excellent interface quality. As the defect density increases beyond approximately 10^{15} cm^{-2}, the EGI values become noticeably higher, reflecting increased energy dissipation cBack contactsed by defect-assisted Shockley–Read–Hall recombination. The largest EGI values are observed for defect densities of 10^{17}–10^{18} cm^{-2}, confirming that severe interface defects significantly reduce the thermodynamic performance of the device. Overall, the results demonstrate that interface defect density has a stronger influence on entropy generation than operating temperature, while the transition near 10^{15} cm^{-2} further confirms the critical interface defect threshold identified from the combined photovoltaic and thermodynamic analyses.

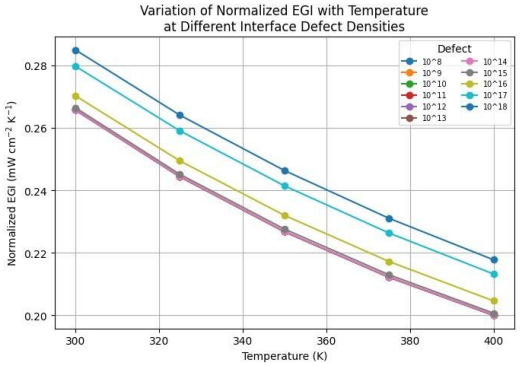

Figure 7: Variation of the Normalized Entropy-Generation Index (EGI) with Operating Temperature at Different SnO_2/$FASnI_3$ Interface Defect Densities

Figure 8(a–b) shows the relationship between the normalized entropy-generation index (EGI) and power conversion efficiency (PCE) under different operating temperatures and SnO_2/$FASnI_3$ interface defect densities. A clear inverse relationship is observed, where higher EGI corresponds to lower PCE. At low interface defect densities (10^8–10^{14} cm^{-2}), the device maintains a high efficiency of about 20–20.6% with low EGI values, indicating minimal irreversible energy losses and effective charge collection. However, once the defect density exceeds approximately 10^{15} cm^{-2}, the EGI increases while the PCE decreases rapidly, confirming

the onset of defect-assisted Shockley–Read–Hall recombination. Although the normalized EGI decreases slightly with increasing temperature due to temperature normalization, the simultaneous reduction in PCE indicates that elevated temperatures still promote non-radiative recombination and performance degradation. Overall, the results reveal a strong negative correlation between EGI and PCE and identify an interface defect density of approximately 10^{15} cm^{-2} as the critical threshold beyond which thermodynamic losses increase significantly. This highlights the importance of interface passivation for achieving high-efficiency and thermally stable $FASnI_3$ perovskite solar cells.

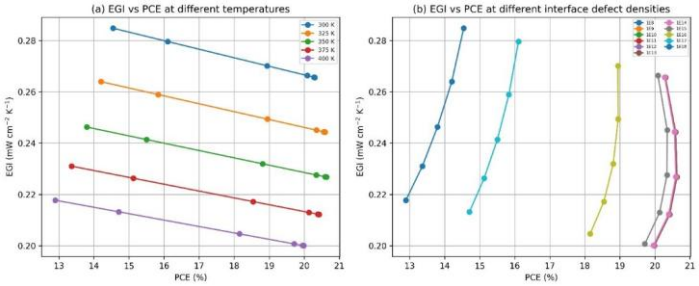

Figure 8: (a) Variation of the Normalized Entropy-Generation Index (EGI) with Power Conversion Efficiency (PCE) at Operating Temperatures of 300, 325, 350, 375, and 400 K. (b) Variation of the Normalized entropy-Generation Index (EGI) with Power Conversion Efficiency (PCE) for $SnO_2/FASnI_3$ Interface Defect Densities Ranging from 10^8 to $10^{18} cm^{-2}$

CONCLUSION

This study investigated the combined effects of operating temperature (300–400 K) and $SnO_2/FASnI_3$ interface defect density (10^8–10^{18} cm^{-2}) on the photovoltaic and thermodynamic performance of an Front contact/$SnO_2/FASnI_3$/CuI/back contact perovskite solar cell using SCAPS-1D simulation. The results show that the device exhibits good thermal stability, maintaining efficiencies close to 20% across the investigated temperature range, with optimum performance at 350 K. In contrast, interface defect density has a much greater impact on device performance. A critical interface defect threshold of approximately 10^{15} cm^{-2} was identified, below which the device operates in a defect-tolerant regime with stable power conversion efficiency, low power loss, and nearly constant normalized entropy-generation index (EGI). Above this threshold, enhanced Shockley–Read–Hall recombination causes rapid deterioration in photovoltaic performance and increased irreversible energy losses. The strong correlation between EGI and photovoltaic degradation demonstrates that the proposed normalized EGI is a useful complementary metric for assessing thermodynamic losses and interface quality. These findings highlight the importance of interface passivation and suggest that maintaining the $SnO_2/FASnI_3$ interface defect density below 10^{15} cm^{-2} is essential for achieving high-efficiency, thermally stable, lead-free $FASnI_3$ perovskite solar cells.

Conflict of Interest Statement

The authors declare that there are no known financial interests, personal relationships, or competing interests that could have influenced the work reported in this paper.

Formatted: Justified, Line spacing: single

REFERENCES

Abbas, M., Xu, X., Rauf, M., & Kyaw, A. K. K. (2024). A comprehensive review on defects-induced voltage losses and strategies toward highly efficient and stable perovskite solar cells. *Photonics*, *11*, 87. https://doi.org/10.3390/photonics11010087

Abdelaziz, S., Zekry, A., Shaker, A., & Abouelatta, M. J. O. M. (2020). Investigating the performance of formamidinium tin-based perovskite solar cell by SCAPS device simulation. *Optical Materials*, *101*, 109738.

Abdulsalam, H., & Lariski, F. M. (2026). Defect and temperature effects in MASnI3 perovskite solar cells: A SCAPS-1D simulation study with interface and recombination analysis. *UMYU Scientifica*, *5*(1), 344–358. https://doi.org/10.56919/usci.2651.029

Afrin, P., Farjana, K., Vumije, A., & Uddin, M. (2024). An investigation on the impact of temperature variation over the performance of formamidinium tin iodide perovskite solar cell using SCAPS simulation. *AIP Advances*, *14*(7). https://doi.org/10.1063/5.0209332

Alahmadi, A. N. (2026). Hole and electron transport layer optimization for highly efficient lead-free MASnI2Br perovskite solar cells: A simulation study. *Crystals*, *16*(3), 174.

Alqurashi, R. S. (2024). Comprehensive investigation of material properties and operational parameters for enhancing performance and stability of FASnI3-based perovskite solar cells. *Scientific Reports*, *14*, Article 16411.

AlZohbi, G. (2026). Materials for solar photovoltaics: A comprehensive review of advancements, challenges, and future directions. *Sustainability*, *18*(12), 5842.

Amusan, O. O., Louis, H., Zafar, S. U., Hamzat, A. T., & Peter, D. M. (2019). Different interface engineering in organic solar cells: A review. *Chemical Methodologies*, *3*, 425–441.

Burgelman, M., Nollet, P., & Degrave, S. (2000). Modelling polycrystalline semiconductor solar cells. *Thin Solid Films*, *361–362*, 527–532.

Burgelman, M., Verschraegen, J., Degrave, S., & Nollet, P. (2004). Modeling thin-film PV devices. *Progress in Photovoltaics: Research and Applications*, *12*(2–3), 143–153.

Dipta, S. S., Rahim, A., & Uddin, A. (2024). Encapsulating perovskite solar cells for long-term stability and prevention of lead toxicity. *Applied Physics Reviews*, *11*(2). https://doi.org/10.1063/5.0197154

El Arfaoui, Y., Khenfouch, M., & Habiballah, N. (2023). Efficient all lead-free perovskite solar cell simulation of FASnI3/FAGeCl3 with 30% efficiency: SCAPS-1D investigation. *Results in Optics*, *13*, 100554.

Green, M. A., Dunlop, E. D., Yoshita, M., Kopidakis, N., Bothe, K., Siefer, G., Hao, X., & Jiang, J. Y. (2025). Solar cell efficiency tables (Version 66). *Progress in Photovoltaics: Research and Applications*, *33*(7), 795–810.

Hanif, M. S., Qasim, I., Malik, M. I., Nasir, M. F., Ahmad, O., & Rashid, A. (2024). Development of low-cost and high-efficiency solar modules based on perovskite solar cells for large-scale applications. *Heliyon*, *10*(4).

Ho, S., Igbokwe, E. E., & Olasanmi, O. O. (2025). Photovoltaic technology: Power conversion efficiency of solar cells. *Asian Journal of Chemistry*, *37*(9), 2092–2114.

Igbokwe, E. E., Nwaokorongwu, E. C., Uchechukwu, A. K., & Emole, E. C. (2026). Defect-dominated performance limits in $FASnI_3$ perovskite solar cells: A thickness-dependent simulation study. *Communication in Physical Sciences*, *13*(5), 763–773.

Islam, B., Khan, T. M., Rahaman, M. M., & Ahmed, S. R. A. (2026). Computational optimization of MASnI3 perovskite solar cells using SCAPS-1D simulations and machine learning techniques. *RSC Advances*, *16*(2), 1172–1192.

Ke, W., Stoumpos, C. C., & Kanatzidis, M. G. (2018). "Unleaded" perovskites: Status quo and future prospects of tin-based perovskite solar cells. *Advanced Materials*, *31*(47), Article 1803230.

Khan, T. M., & Ahmed, S. R. A. (2024). Investigating the performance of FASnI3-based perovskite solar cells with various electron and hole transport layers: Machine learning approach and SCAPS-1D analysis. *Advanced Theory and Simulations*, *7*(10), 2400353.

Kojima, A., Teshima, K., Shirai, Y., & Miyasaka, T. (2009). Organometal halide perovskites as visible-light sensitizers for photovoltaic cells. *Journal of the American Chemical Society*, *131*(17), 6050–6051.

Li, X., Long, F., Gao, Y., Xu, H., Qin, J., Yu, F., & Yao, D. (2026). Interface engineering for inverted perovskite solar cells via cooperative passivation of bimolecular additives to achieve low voltage loss. *Small*, e12467. https://doi.org/10.1002/smll.202512467

Lin, L., & Ravindra, N. M. (2020). Temperature dependence of CIGS and perovskite solar cell performance: An overview. *SN Applied Sciences*, *2*(8). https://doi.org/10.1007/s42452-020-3169-2

Meng, Q., Chen, Y., Xiao, Y. Y., Sun, J., Zhang, X., Han, C. B., & Yan, H. (2021). Effect of temperature on the performance of perovskite solar cells. *Journal of Materials Science: Materials in Electronics*, *32*(10), 12784–12792.

Moot, T., Boyd, C. C., Parilla, P. A., Rosales, B. A., Wolf, E. J., Wheeler, L. M., & Luther, J. M. (2021). Temperature coefficients of perovskite photovoltaics for energy yield calculations. *ACS Energy Letters*, *6*(5), 2038–2047. https://doi.org/10.1021/acsenergylett.1c00748

Nelson, J. A. (2003). *The physics of solar cells*. World Scientific Publishing Company.

Noman, M., Khan, A. D., Khan, A. H. H., & Jan, S. T. (2024). Interface engineering and defect passivation for enhanced hole extraction, ion migration, and optimal charge dynamics in both lead-based and lead-free perovskite solar cells. *Scientific Reports*, *14*(1). https://doi.org/10.1038/s41598-024-56246-4

Peng, L., & Xie, W. (2020). Theoretical and experimental investigations on the bulk photovoltaic effect in lead-free perovskites MASnI3 and FASnI3. *RSC Advances*, *10*(25), 14679–14688. https://doi.org/10.1039/d0ra02584d

Savill, K. J., Ulatowski, A. M., & Herz, L. M. (2021). Optoelectronic properties of tin–lead halide perovskites. *ACS Energy Letters*, *6*, 2413–2426. https://doi.org/10.1021/acsenergylett.1c00776

Tai, Q., Cao, J., Wang, T., & Yan, F. (2019). Recent advances toward efficient and stable tin-based perovskite solar cells. *EcoMat*, *1*(1), Article e12004.

Wang, M., Wang, W., Ma, B., Shen, W., Liu, L., Cao, K., & Huang, W. (2021). Lead-free perovskite materials for solar cells. *Nano-Micro Letters*, *13*(1), 62.

Wang, Z., Gao, H., Wu, D., Meng, J., Deng, J., & Cui, M. (2024). Defects and defect passivation in perovskite solar cells. *Molecules*, *29*, 2104. https://doi.org/10.3390/molecules29092104

Wu, Y., Wang, D., Liu, J., & Cai, H. (2021). Review of interface passivation of perovskite layer. *Nanomaterials*, *11*, 775. https://doi.org/10.3390/nano11030775

Yao, H., Zhou, F., Li, Z., Ci, Z., & Ding, L. (2020). Strategies for improving the stability of tin-based perovskite (ASnX3) solar cells. *Advanced Science*, *7*(10), Article 1903540.

Zhang, Q., Hao, F., Li, J., Zhou, Y., Wei, Y., & Lin, H. (2018). Perovskite solar cells: Must lead be replaced—and can it be done? *Science and Technology of Advanced Materials*, *19*(1), 425–442.

Zhang, W., Li, G., & Chen, K. (2026). Improving the performance of lead-free perovskite solar cells. *Communications Materials*, *7*, 189. https://doi.org/10.1038/s43246-026-01277-9